3D CAFE simulation of a macrosegregation benchmark experiment

Tommy Carozzani, Hugues Digonnet, Michel Bellet, Charles-André Gandin

3D CAFE simulation of a macrosegregation benchmark experiment

T. Carozzani[1], H. Digonnet[1], M. Bellet[1], Ch.-A. Gandin[1,2]
[1]MINES ParisTech & [2]CNRS, CEMEF UMR 7635, 06904 Sophia Antipolis, France

E-mail: Charles-Andre.Gandin@mines-paristech.fr

Abstract. A macrosegregation benchmark experiment is simulated using a three dimensional (3D) Cellular Automaton (CA) - Finite Element (FE) model. It consists of a Sn - 3 wt% Pb alloy solidified in a rectangular cavity. Thanks to tabulated thermodynamic properties and solidification paths with temperature and composition, the effect of natural convection and macrosegregation on cooling curves is correctly predicted. Nucleation parameters are adjusted so that the simulated grain structure correlates with the real grain structure. Although macrosegregation is well predicted, this is not the case for freckles yet observed in the solidified sample.

1. Introduction

Macrosegregation is a major problem for the casting industry. It can be due to several mechanisms involving *i*- solute transport in the liquid and in the mushy zone due to fluid flow, *ii*- grain transport because of gravity and convection, *iii*- liquid flow driven by shrinkage and deformation and *iv*- diffusion of solute in the liquid and solid phases [1].

Due to the multiple and overlapping origins of macrosegregation, quantitative validation of simulation tools is a challenging task. Experimental benchmarks have thus been developed for that purpose. A reference work is the early experiment of Hebditch and Hunt [2] in Pb - 48 wt% Sn alloy. A similar benchmark was recently developed with enhanced data acquisitions and metallurgical inspections [3, 4]. It provides detailed data on temperature evolution during solidification and measured distribution of composition and eutectic fraction in the solidified ingot. Alloy composition can also be changed and forced convection can be studied thanks to electromagnetic stirring. Few attempts have already been made to simulate the experiment (e.g. [5, 6]). However, they lack either tracking of the columnar grain structure and/or 3D considerations. Both are yet expected to have a great influence on the results if quantitative comparison is to be reached. We propose here to simulate such a benchmark experiment with a CAFE model that accounts for structure and macrosegregation in three dimensions.

2. Experimental

A Sn - 3 wt% Pb ingot is considered. Its dimensions are 10 cm width x 6 cm height x 1 cm thick. The opposite smallest surfaces, dimensions 6 cm x 1 cm, are positioned vertically in contact with heat exchangers that serve to melt or freeze the ingot by imposed temperature evolutions. The other sides of the ingot are well insulated and considered as adiabatic. The ingot is first melted by heating up to 260 °C. A 10 minutes holding time at this temperature is applied in order to homogenize the liquid while imposing a forced convection by electromagnetic stirring. Stirring is then stopped and time is reset to zero. The right-hand-side (RHS) heat exchanger is heated up to 280 °C while the left-hand-

side (LHS) heat exchanger is cooled down to 240 °C. These temperatures are maintained for 1000s so that natural convection due to the temperature difference is stabilized. Finally, the RHS and LHS heat exchangers are simultaneously cooled down at -0.03 °C s^{-1} until complete solidification, so that a 40 °C difference is maintained between the LHS and RHS heat exchangers.

Temperature evolution is recorded with 50 thermocouples equally spaced by 1 cm in a regular lattice of 5 rows x 10 columns, plus 6 thermocouples in each heat exchanger. The segregation map is retrieved with X-ray imaging and quantitative chemical analyses using Inductively Coupled Plasma (ICP) spectrometry at the same 50 positions where the thermocouples are located. Experimental results presented in the next section are based on reference 4.

3. Modeling

3.1. FE method

The CAFE model has been extensively described elsewhere [7-10] and is only briefly presented hereafter. It consists of a standard FE method to solve average macroscopic equations written with the approximation of constant and equal densities for both solid and liquid phases, ρ_0, as well as a fixed solid phase.

The following set of equations is solved to compute the average enthalpy, $\langle H \rangle$, the average composition, $\langle w \rangle$, and the average velocity, $\langle \mathbf{v} \rangle$.

Energy conservation
$$\rho_0 \left(\frac{\partial \langle H \rangle}{\partial t} + \langle \mathbf{v} \rangle \cdot \nabla \langle H^l \rangle^l \right) - \nabla \cdot \left(\langle \kappa \rangle \nabla T \right) = 0 \quad (1)$$

Solute conservation
$$\frac{\partial \langle w \rangle}{\partial t} + \langle \mathbf{v} \rangle \cdot \nabla \langle w^l \rangle^l - \nabla \cdot \left(D^l g^l \nabla \langle w^l \rangle^l \right) = 0 \quad (2)$$

Momentum conservation
$$\rho_0 \frac{\partial \langle \mathbf{v} \rangle}{\partial t} + \frac{\rho_0}{g^l} \nabla \cdot \left(\langle \mathbf{v} \rangle \times \langle \mathbf{v} \rangle \right) = \nabla \cdot \left(\mu \nabla \langle \mathbf{v} \rangle \right) - g^l \nabla p + g^l \rho \, \mathbf{g} - \mathbf{M} \quad (3)$$

where $\langle H^l \rangle^l$, $\langle \mathbf{v} \rangle$, $\langle \kappa \rangle$ and T are respectively the average liquid enthalpy, the average liquid velocity, the average thermal conductivity and the temperature, $\langle w^l \rangle^l$, D^l and g^l are respectively the average liquid composition, the diffusion coefficient of the solutal element in the liquid and the volume fraction of liquid, μ, p and **g** are the dynamic viscosity, the intrinsic pressure in the liquid and the gravity vector. Diffusion in the solid is neglected here. The Boussinesq approximation is assumed in order to compute the fluid flow induced by natural convection. The density is therefore kept constant in all terms of the momentum equation except in the gravity term, where:

$$\rho = \rho_0 \left(1 - \beta_T \left(T - T_0 \right) - \beta_w \left(\langle w^l \rangle^l - w_0^l \right) \right) \quad (4)$$

with β_T and β_w the thermal and solutal expansion coefficients, T_0 and w_0^l reference temperature and composition. The volumetric friction force, **M**, accounts for the interaction of the liquid with the solid phase. It is defined as $\mathbf{M} = (\mu/K) \, g^l \langle \mathbf{v} \rangle$ with the local permeability given by $K = [g^{l\,3} \lambda_2^{\,2}] / [180 \, (1-g^l)^2]$. In the fully liquid region, K tends toward infinity and the classical Navier-Stokes equation is retrieved. In the solid region, K tends toward zero and the **M** term becomes dominant, leading to Darcy's relation. Details on the calculation of the permeability are given elsewhere [8]. It mainly depends on the secondary dendrite arm spacing, λ_2. The value used in the present work is directly extracted from measurements [4]. Finally, a local solidification model is used, that predicts the liquid fraction and the temperature considering an average enthalpy and an average composition, while accounting for the nucleation and growth the grain structure with some undercooling [10]. This is explained hereafter.

3.2. CA method

A regular grid of cubic cells is generated in the simulation domain, with a cell size smaller than the FE mesh. Random cells are picked where nucleation sites are allocated. A critical nucleation undercooling,

ΔT_{nucl}, is associated to each site. Its value is randomly chosen following a Gaussian distribution defined by a mean undercooling, ΔT_N, a standard deviation, ΔT_σ, and the total density n_{max} that corresponds to the integral of the distribution. If the CA cell associated with the nucleation site is still liquid when the local undercooling reaches the nucleation undercooling, then the site nucleates a new grain with a random orientation given by a set of Euler angles.

A velocity, v_p, is used to compute the growth of the half diagonals of a local octahedral shape associated with the CA cell. These diagonals corresponds to the main <100> dendrite growth directions of a cubic metal. For a cell located at the grain boundary with the free liquid, the supersaturation, Ω, is proportional to the difference between the dendrite tip composition, w^{ls}, and the average liquid composition far from the interface, $w^{l\infty}$, the latter being approximated as <w>:

$$\Omega = (w^{ls} - w^{l\infty})/(w^{ls} (1-k)) \quad (5)$$

It is computed from a boundary layer correlation:

$$\Omega = P_{v_p} \exp(P_{v_p}) \{E_1(P_{v_p}) - E_1(P_{v_p} [1 + 4 (A\, Re_{2r}^B\, Sc^C \sin(\theta/2))^{-1}])\} \quad (6)$$

with $A = 0.5773$, $B = 0.6596$, $C = 0.5249$ and where $P_{v_p} = (r\, v_p)/(2D^l)$ is the growth Péclet number defined with the dendrite tip radius r, $P_{vl} = (r\, v^l)/(2D^l)$ is the flow Péclet number proportional to the liquid velocity, v^l, $Sc = \nu/D^l$ is the Schmidt number defined with the kinematic viscosity ν, $Re_{2r} = 4P_{vl}/Sc$ is the Reynolds number, θ is the angle between the fluid flow direction and a <100> growth direction [11]. The velocity of the dendrite tip is computed with the relation given by the marginal stability criterion:

$$r^2 v_p = (D^l/\sigma^*) (\Gamma/(m_L (k-1) w^{ls}) \quad (7)$$

with m_L the liquidus slope, k the segregation coefficient, Γ the Gibbs-Thomson coefficient and σ^* the stability constant equal to $(4\pi^2)^{-1}$ [8, 9]. The volume fraction of the propagated growth front, $g^{(i)}$, is then computed for each cell from the growing shape. $g^{(i)}$ locally accounts for the presence of structure i, here dendritic (i=1) or eutectic (i=2) for a binary Sn-Pb alloy [10]. When only the dendritic structure is present, the value $g^{(1)}=0$ corresponds to a fully liquid state. The value $g^{(1)}=1$ corresponds to a "fully mushy" state, i.e. the remaining liquid is interdendritic. Intermediate values correspond to a transition state made of mixture of a mushy zone, $g^{(1)}$, plus an extradendritic liquid, $1-g^{(1)}$. Thus the value of $g^{(1)}$ depends on nucleation events, growth kinetics, and more generally temperature evolution in the ingot in the vicinity of the FE nodes. As no growth is solved here for the eutectic structure, $g^{(2)}$ is simply set to one below the eutectic temperature, T_E.

3.2. Coupling with thermodynamic

Summation of $g^{(i)}$ over the CA cells permits to access the average information at the FE nodes. It is used by a microsegregation model for the determination of the internal phase fractions in the primary and secondary structures at the FE nodes. For that purpose, a relation between enthalpy, average composition and temperature is needed in the energy conservation [10]. The microsegregation model is based here on a tabulation of the hypoeutectic phase diagram assuming the lever rule approximation. Enthalpy of different phases α, $H^{(\alpha)}$, and internal fractions for each phase in each structure, $g_i^{\alpha_i^{(i)}}$, are tabulated for several average solute composition, <w> and temperature, T. Given the local composition from the solution of the solute mass conservation, <w>, the average enthalpy from the energy conservation, <H>, and the volume fractions of structures from the CA resolution, $g^{(i)}$, a local temperature, T, and internal phase fractions, $g_i^{\alpha_i^{(i)}}$, verify the relation:

$$<H> = \sum_{\alpha_i} g^{(i)}\, g_i^{\alpha_i^{(i)}}(<w>,T)\, H^{\alpha}(<w>,T) \quad (8)$$

where $H^{\alpha}(<w>,T))$ and $g^{\alpha_i^{(i)}}(<w>,T)$ are computed by linear interpolations of the tabulations. Variations of heat capacities and latent heat with temperature and composition are thus implicitly taken into account, as well as possible solid phase transformations. Figure 1 illustrates the tabulation of the enthalpy and internal fraction of phases as a function of temperature in the dendritic and eutectic structures for various Pb compositions of hypoeutectic Sn-Pb alloys. As read on figure 1b, solidification takes place with a primary dendritic structure made of the BCT_A5 phase which is partially transformed into the FCC_A1 phase when the solvus temperature is reached. The later solid state phase transformation and its temperature depend on the local average composition.

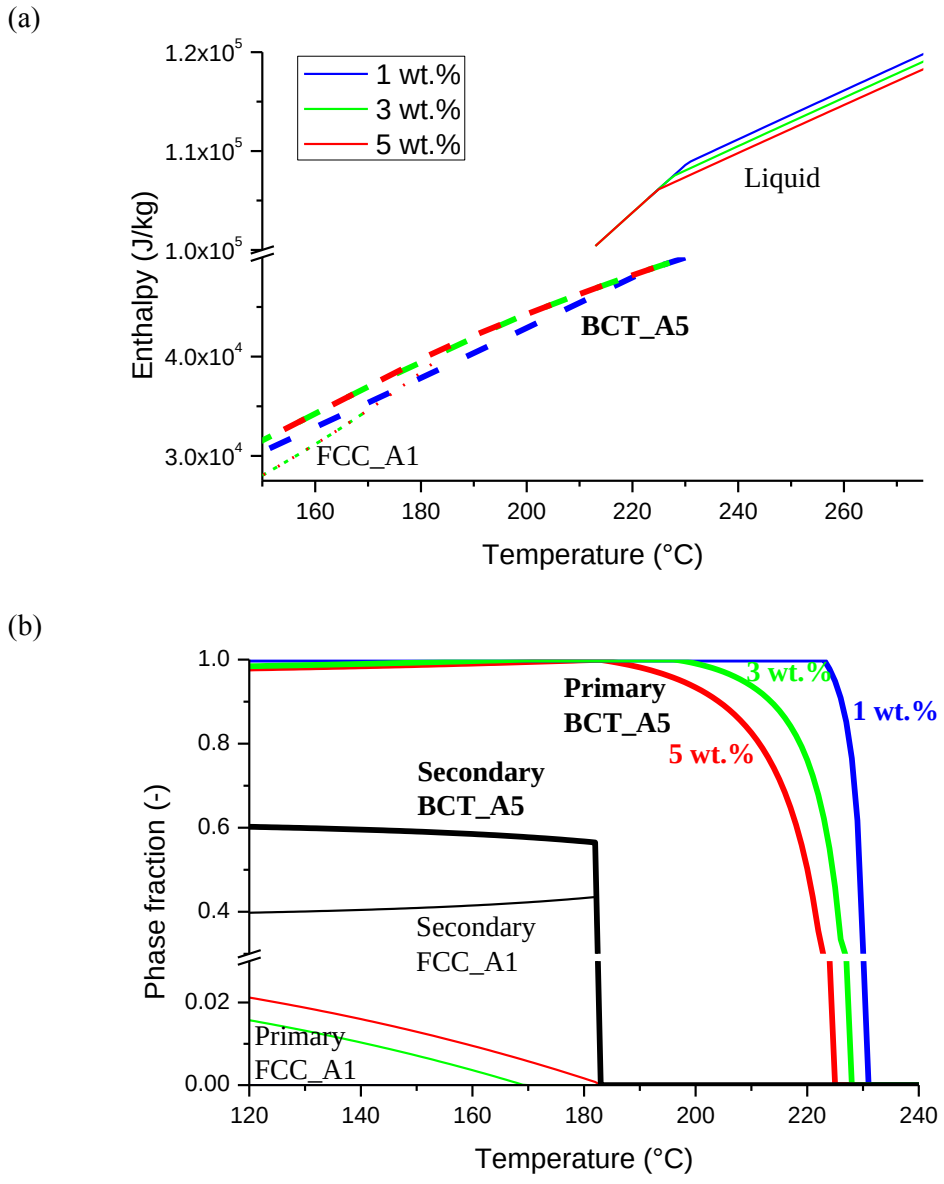

Figure 1. Tabulated (a) enthalpy and (b) internal phase fractions for (colored lines) the primary dendritic structure and (black lines) the secondary eutectic structure as a function of temperature and Pb composition. Internal phases are (thick lines) BCT_A5 and (thin lines) FCC_A1. Data extracted from the PBIN database using ThermoCalc and assuming full equilibrium.

The eutectic structure is made of a mixture of the BCT_A5 and FCC_A1 phases with internal fractions also changing with temperature. Please note that these phase names are directly extracted from the PBIN database. The present tabulation permits to account for solid state transformations, although it is not clear if they are made possible due to the limited diffusion of solute in the solid phases. This strategy of coupling yet clearly permits to be as close as possible to thermodynamic properties, thus directly using tabulated enthalpies for each phase as a function of temperature and composition as shown on figure 1a. The method that consists of an extraction of heat capacity and latent heat as a function of temperature is avoided. Material properties become dependent on alloy composition and phase fractions, the later being considerably changed due to macrosegregation. Such methodology was shown earlier to provide advantages when quantitative comparison with measurements is to be reached [12].

4. Results and discussion

The global mass conservation requires adiabatic conditions at the boundaries of the simulation domain. A zero flow velocity is also imposed on ingot's boundaries. For heat transfer, all boundaries are adiabatic except the small right and left surfaces in contact with the heat exchangers. Temperatures that are imposed on these boundaries are deduced from the heat flow in the heat exchangers and the temperature in the sample near the surface [4]. This heat flow is deduced from temperature measurements in the heat exchanger at a given height. Thermocouples positions are given elsewhere [4]. For the results presented hereafter, the selected positions are distributed in the length of the ingot, as positions 5, 35, 65 and 95 mm from LHS of the ingot surface and at mid-height, i.e. at 30 mm from the ingot base. These positions are referred to as L30, L27, L24 and L21 in the following, respectively. Temperature evolutions at mid-height on left and right sides, i.e. at 0 and 100 mm from the left side of the ingot surface deduced from the heat flow analysis in the heat exchangers at mid-height, are referred to as positions $FL3_{in}$ and $FR3_{in}$, respectively. Simulation parameters are given in table 1. Note that the liquidus slope, m_L, and the partition coefficient, k, are only used to compute the velocity of the growth front with the CA model because coupling with thermodynamic properties deduced from the PBIN database have not yet been implemented.

Figure 2 presents the simulated fluid velocity at different times, along with the computed grain structure. As expected, the interaction between the flow and the structure is very strong. Although it is not visible on figure 2, fluid flow within the mushy zone is not null. It is however much lower than in the free liquid. The convection loop seen prior to solidification, e.g. before 2400 s in figure 2, is mainly induced by the temperature difference between the LHS and RHS heat exchangers. Figure 3 permits to access the imposed time evolution of the corresponding boundaries thanks to the reported temperature history at the ingot surfaces $FL3_{in}$ and $FR3_{in}$. Starting from an initial liquid melt at around 260 °C, the LHS of the ingot is heated up and hold at around 273 °C while the RHS is cooled down and hold at around 243 °C. The 30 °C difference between the LHS and RHS deviates from the desired 40 °C difference imposed between the heat exchangers. This is due to the heat resistance between the heat exchangers and the alloy. Upon further cooling, the grain structure develops. The size of the free liquid is further decreased. At about 3300 s, while half of the sample is still fully liquid, no more superheat remains and the temperature gradient is almost zero, further dumping convection.

Predicted and experimental cooling curves are shown in figure 3, together with the predicted solid fraction at the same locations. The agreement between measured and simulated cooling curves is overall very good. During the first stages of the experiment ($t < 1600$s), the temperature gradient is well represented. No numerical oscillations are observed, which confirms that fluid convection reaches a stable state. This could not be reached in two-dimensional simulations: the fluid flow was more pronounced and no permanent regime could be achieved, leading to perturbed cooling curves with no clear temperature plateau. During solidification ($2000\text{s} < t < 4000\text{s}$), all abrupt inflexions on the cooling curves are also retrieved. They correspond to the change from a fully liquid to fully mushy state when the dendritic front overgrows the thermocouple position. An interesting slope change is retrieved shortly after time 3500 s on thermocouple L21. From the CAFE simulation, it can be interpreted as a

recalescence linked with a sudden increase of the solid fraction. It is due to the nucleation of equiaxed grains in the melt taking place at this location while temperature is almost uniform leading to a fast grain growth and latent heat released sufficient to increase the temperature. This phenomenon can be observed on figure 2c where few grains have nucleated in the melt, and the columnar grain interface is destabilized due to an almost uniform temperature as well as a fully undercooled liquid.

As shown in figure 4, the simulated grain structure can also be compared with the experimental macrograph. The structure is mainly columnar and the trend for the grains to tilt upward is reproduced by the simulation. Explanation is due to the introduction of the fluid flow direction with respect to the <100> growth directions of the grains for the computation of the growth kinetic. Because the flow is going downward along the growth front, as is shown in Fig. 2b, the growth directions of the grains that are opposite to the flow can adopt a smaller undercooling. They extend faster in the undercooled liquid and lead to the present grain selection. While this correlates well with the experimental observations, the grain direction does not retrieve the strong misorientation. It is not obvious whereas this is due to the kinetic law itself, or to the growth algorithm implemented in the CA method. Further investigations should be led in this direction that would probably require more dedicated experiments. Adjustments have been made to the nucleation parameters (table 1) in order to fit the observed grain density, allowing correct prediction of the columnar-to-equiaxed (CET) transition.

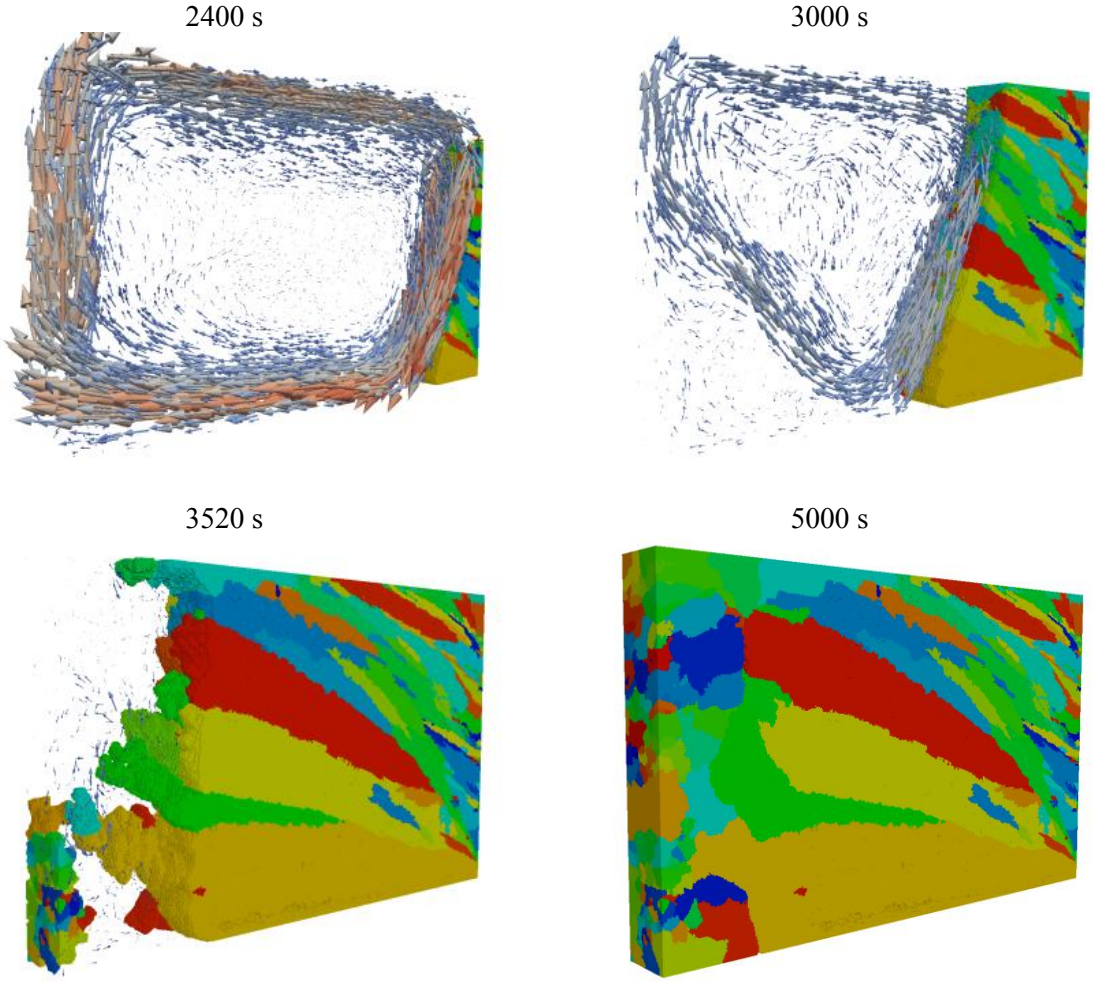

Figure 2. Predicted fluid flow and grain structure at different times of a 3D CAFE simulation.

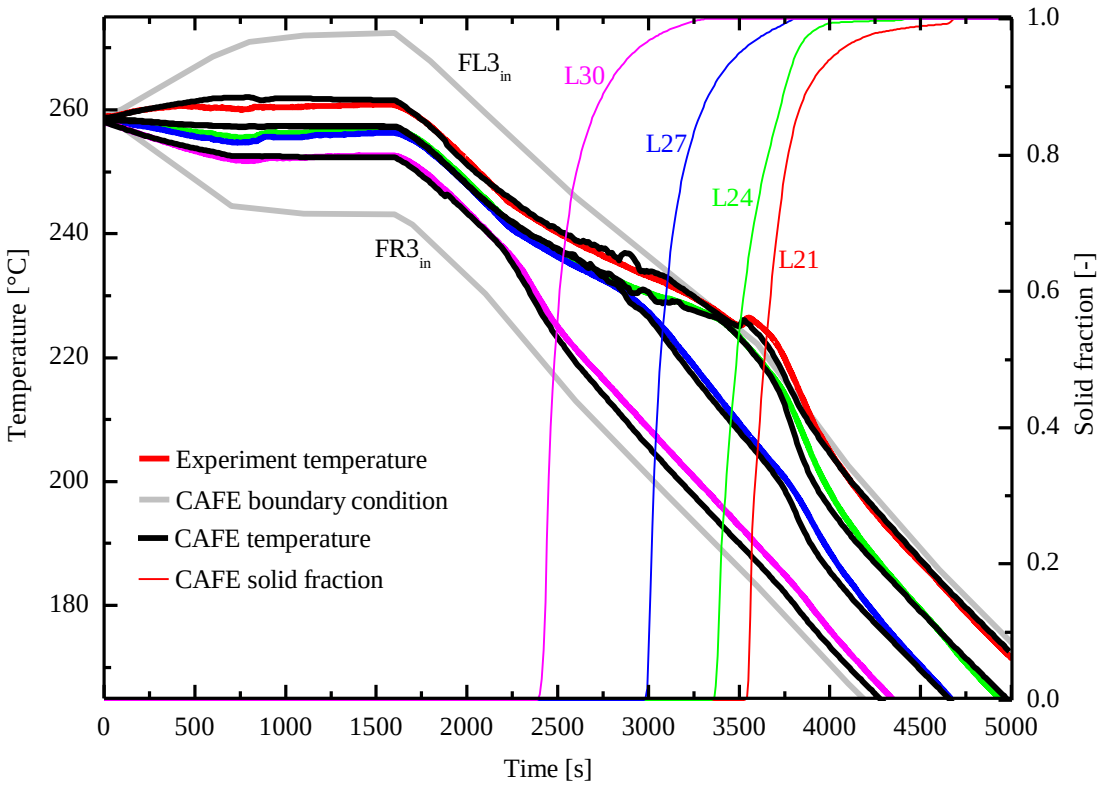

Figure 3. Experimental [4] (thick black lines) and predicted (thick colored lines) cooling curves, along with predicted solid fraction (thin lines). Curves are given for four positions L21, L24, L27 and L30, which are respectively at 5, 35, 75 and 95mm from the left side, at ingot's mid-height. Imposed temperatures at mid-height on right, $T(FR3_{in})$, and left, $T(FL3_{in})$, sides are also represented.

Figure 5 shows the predicted solute composition maps. The measured distribution is deduced from quantitative chemical analysis. The CAFE prediction is drawn at the ingot center with the same scale. Only the area delimited with the black rectangle can be compared. It corresponds to the measurements area. The global agreement in the right part of the ingot is good, as the chemical analysis would correspond to a mean value, i.e. within the thickness of the sample. In the left part of the ingot, a highly segregated zone is predicted that crosses almost all the ingot's height, whereas it is only measured at the bottom of the ingot. However, it is believed that measurements are not conducted on a sufficiently dense array. A better way to conduct comparison would then be to average the predicted quantities over a volume that is representative of the quantitative measurement.

A X-ray image of the ingot reveals segregated channels in the bottom-right part of the ingot [4]. This is not predicted by the simulation. Although the reason for this discrepancy is not yet very clear, anisotropy of the mush permeability is suspected to play a role, while it is only treated as isotropic in the present model. Freckles prediction also strongly depends on the mesh size [6]. Despite many numerical optimizations [9] and parallel computing, the current 3D simulation requires heavy resources thus limiting the minimum element size (table 1).

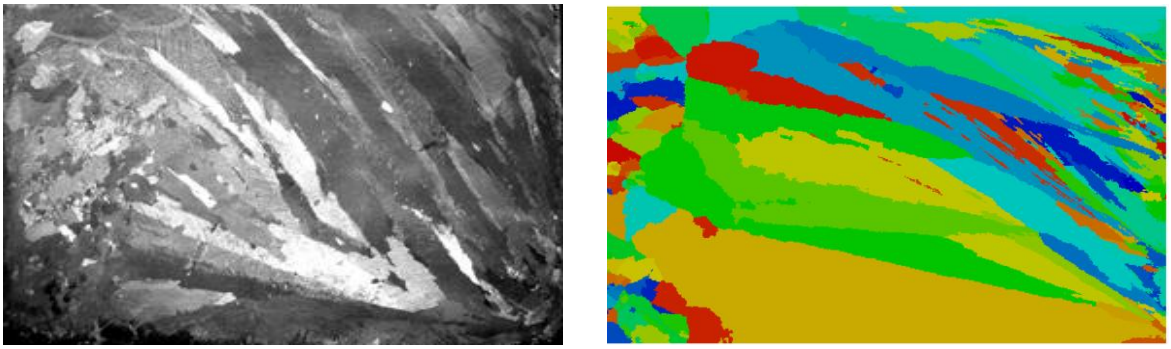

(a) (b)

Figure 4. Grains structure at ingot center (a) as observed by metallographic etching [4] and (b) as predicted by the 3D CAFE model.

5. Conclusion

A 3D CAFE model was presented and applied to macrosegregation benchmark experiment. It is able to retrieve measured cooling curves, macrosegregation and grain structure. Quantitative prediction being mainly achieved when comparing temperature evolution, it is believed that the fluid flow and growth undercooling are also well reproduced. However, prediction of segregated channel is still disappointing and may require additional resources and model improvements.

Acknowledgements

This work was funded by the Agence Nationale de la Recherche under projects SMACS and Si-X.

References

[1] Beckermann C 2002 *International Materials Reviews* **47** 243
[2] Hebditch D J and Hunt J D 1974 *Metall. Trans.* **5** 349
[3] Wang X D and Fautrelle Y 2009 *Int. J. Heat and Mass Transfer* **52** 5624
[4] Hachani L, Saadi B, Wang X D, Nouri A, Zaidat K, Belgacem Bouzida A, Ayouni-Derouiche L, Raimondi G and Fautrelle Y 2012 *Int. J. Heat and Mass Transfer* **55** 1986.
[5] Gandin Ch-A, Blaizot J, Mosbah S, Bellet M, Zimmermann G, Sturz L, Browne D J, McFadden S, Jung H, Billia B, Mangelinck N, Nguyen Thi H, Fautrelle Y and Wang X 2010 *Mater. Sci. Forum* **649** 189
[6] Combeau H, Bellet M, Fautrelle Y, Gobin D, Rady M, Arquis E, Budenkova O, Dussoubs B, Duterrail Y, Kumar A, Gandin C A, Goyeau B, Mosbah S and Zaloznik M 2011 *Model. of Casting, Welding and Adv. Solidif. Proc. XIII* (these proceedings)
[7] Gandin Ch-A, Desbiolles J L, Rappaz M and Thevoz Ph 1999 *Metall. Mater. Trans.* A **30** 3153
[8] Guillemot G, Gandin Ch-A and Combeau H 2006 *ISIJ International* **46** 880
[9] Mosbah S, Bellet M and Gandin Ch-A 2010 *Metall. Mater. Trans.* A **41** 651
[10] Carozzani T, Digonnet H and Gandin Ch-A 2012 *Modelling Simul. Mater. Sci. Eng.* **20** 015010
[11] Gandin Ch-A, Guillemot G, Appolaire B and Niane N T 2003 *Mater. Sci. Eng.* A **342** 44
[12] Tourret D, Gandin Ch-A, Volkmann T, Herlach D M 2011 *Acta Mater*. **59** 4665

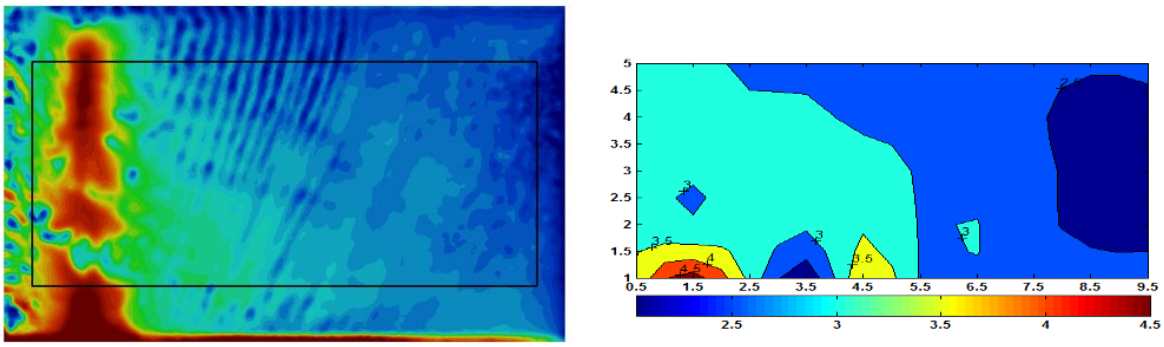

(a) (b)

Figure 5. Segregation map (a) predicted at the center of the ingot and (b) measured by chemical analysis [4]. The black rectangle in (a) corresponds to the measured area represented in (b).

Table 1. Value of simulation parameters.

Parameter	Variable	Value	Unit
Melting temperature	T_m	232.	°C
Eutectic temperature	T_e	183.	°C
Nominal composition	w_0	3.0	wt%
Eutectic composition	w_e	38.0	wt%
Segregation coefficient	k	0.0656	wt%
Liquidus slope	m_L	-1.2895	wt%
Gibbs-Thomson coefficient	Γ	$2. \cdot 10^{-7}$	°C m
Diffusion of Pb in liquid Sn	D^l	$3. \cdot 10^{-9}$	$m^2\ s^{-1}$
Dynamic viscosity	μ^l	$2 \cdot 10^{-3}$	Pa s
Solutal expansion coefficient	β_w	$-5.3 \cdot 10^{-3}$	$wt\%^{-1}$
Thermal expansion coefficient	β_T	$9.5 \cdot 10^{-5}$	$°C^{-1}$
Reference temperature	T_0	228.14	°C
Reference composition	w_0^l	3.0	wt. %
Density	ρ_0	7130	$kg\ m^{-3}$
Gravity field	**g**	-9.81	$m\ s^{-2}$
Thermal conductivity in the solid	κ_s	55	$W\ m^{-1}\ °C^{-1}$
Thermal conductivity in the liquid	κ_l	33	$W\ m^{-1}\ °C^{-1}$
Secondary dendrite arm spacing	λ_2	$90 \cdot 10^{-6}$	m
Maximum nucleation density	n_{max}	10^7	m^{-3}
Average nucleation undercooling	ΔT_n	5.	°C
Nucleation undercooling standard deviation	ΔT_σ	1.	°C
CA cell size		$200 \cdot 10^{-6}$	m
FE mesh size		$780\text{-}1200 \cdot 10^{-6}$	m
Time step		0.1	s
Initial temperature		260.	°C
Initial composition		3.0	wt%
Initial velocity		0.	$m\ s^{-1}$